Supporting Information

Electrochemical and optical detection and machine learning applied to images of genosensors for diagnosis of prostate cancer with the biomarker PCA3

Valquiria C. Rodrigues[1,2], Juliana C. Soares[2], Andrey C. Soares[3], Daniel C. Braz[2], Matias Eliseo Melendez[4,9], Lucas C. Ribas[5], Leonardo F. S. Scabini[2], Odemir M. Bruno[2], Andre Lopes Carvalho[4], Rui Manuel Vieira Reis[4,6,7], Rafaela C. Sanfelice[8], Osvaldo N. Oliveira Jr*[2]

Corresponding Author: chu@ifsc.usp.br

1 Department of Materials Engineering, Sao Carlos School of Engineering, University of Sao Paulo, São Carlos, SP,13563-120, Brazil.
2 Sao Carlos Institute of Physics, University of Sao Paulo, 13566-590 São Carlos, Brazil
3 National Laboratory of Nanotechnology for Agribusiness (LNNA), Embrapa Instrumentation, 13560-970 São Carlos, Brazil.
4 Molecular Oncology Research Center, Barretos Cancer Hospital, 14784-400 Barretos, Brazil.
5 Institute of Mathematics and Computer Science, University of Sao Paulo, Sao Carlos, Brazil
6 Life and Health Sciences Research Institute (ICVS), School of Medicine, University of Minho, Braga, Portugal.
7 ICVS/3B's - PT Government Associate Laboratory, Braga/Guimarães, Portugal.
8 Department of Chemical Engineering, Federal University of the Triângulo Mineiro, Uberaba-MG, Brazil.
9 Pelé Little Prince Research Institute, Little Prince College, Little Prince Complex Curitiba, 80250-060, Curitiba, PR, Brazil.

The spectra for the solutions display a typical band at 510 nm and 520 nm in Figures S1a and S1b, respectively. They confirm the presence of nanoparticles in the solution, with the band intensity tending to stabilize after 75 min. In the presence of chondroitin sulfate (Figure S1b) the band is less intense and wider than expected because chondroitin sulfate protects the nanoparticles[45]. The concentration is crucial to obtain particles with different diameters, since with the reduction gold nanoparticles begins to agglomerate. As stabilizing agents, chondroitin sulfate molecules are located around the nanoparticles, preventing uncontrolled growth. By increasing the concentration of chondroitin sulfate, agglomeration is hampered and smaller nanoparticles form.

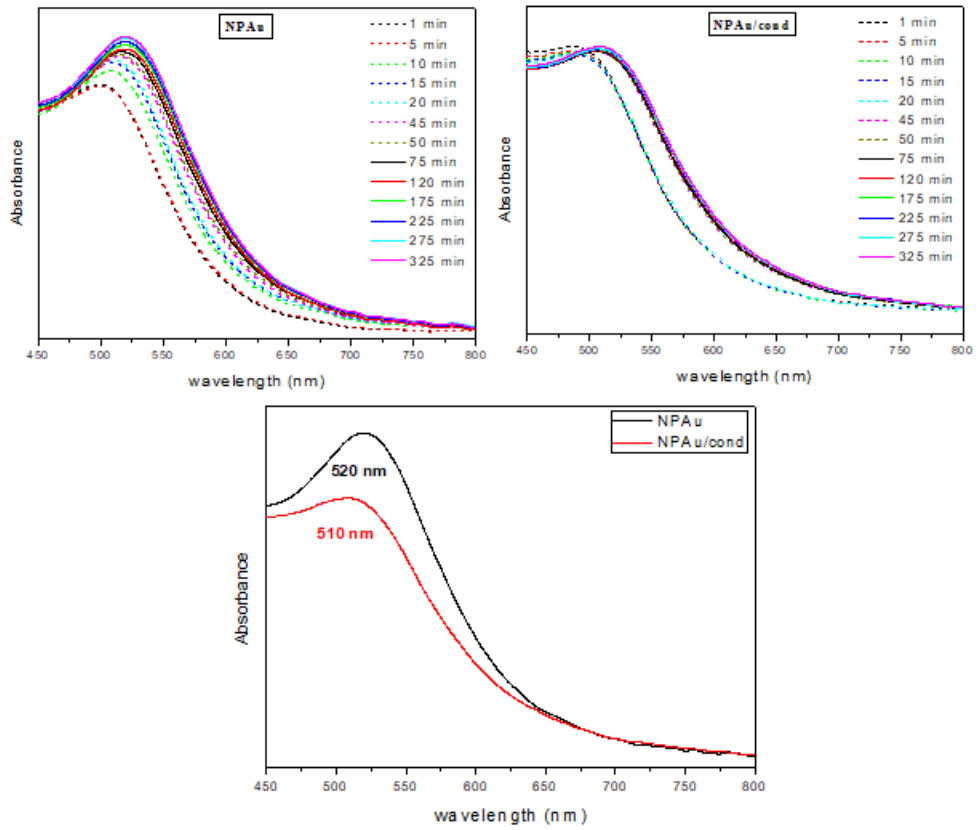

Figure S1 - UV-Vis spectra for aqueous nanoparticle suspensions at distinct times after starting the synthesis: (a) with Chondroitin Sulfate, (b) without chondroitin Sulfate. (c) comparison with the spectra at 75 min from a and b.

a)

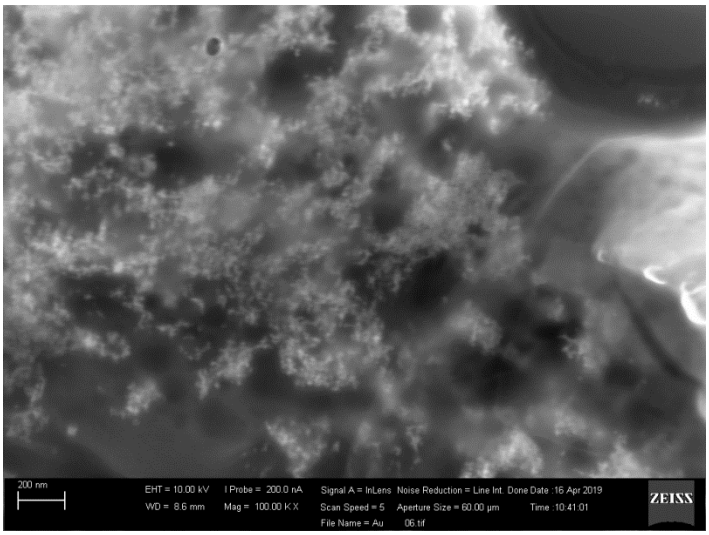

b)

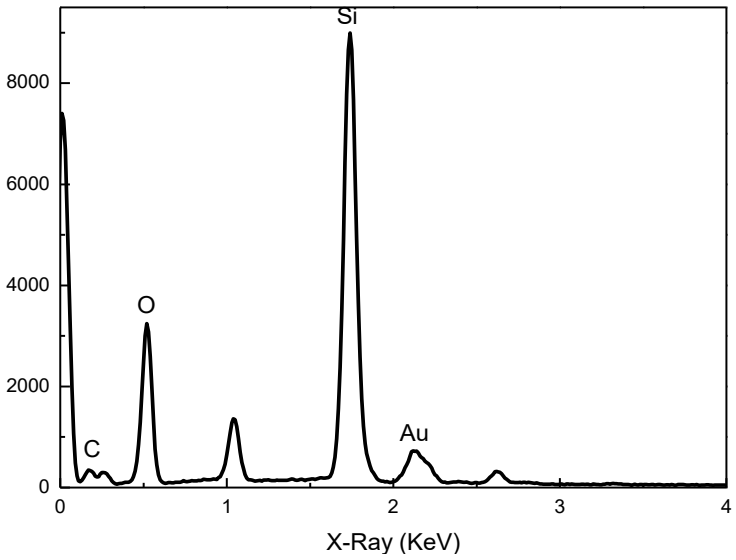

Figure S2. (a) Scanning Electron Microscopy (SEM) of gold nanoparticles and (b) EDX spectrum of chondroitin sulfate synthesized gold nanoparticles.

Table S1. List of EDX Bands

Element	X-rays (keV)
carbon	0.27
oxygen	0.52
gold	2.12

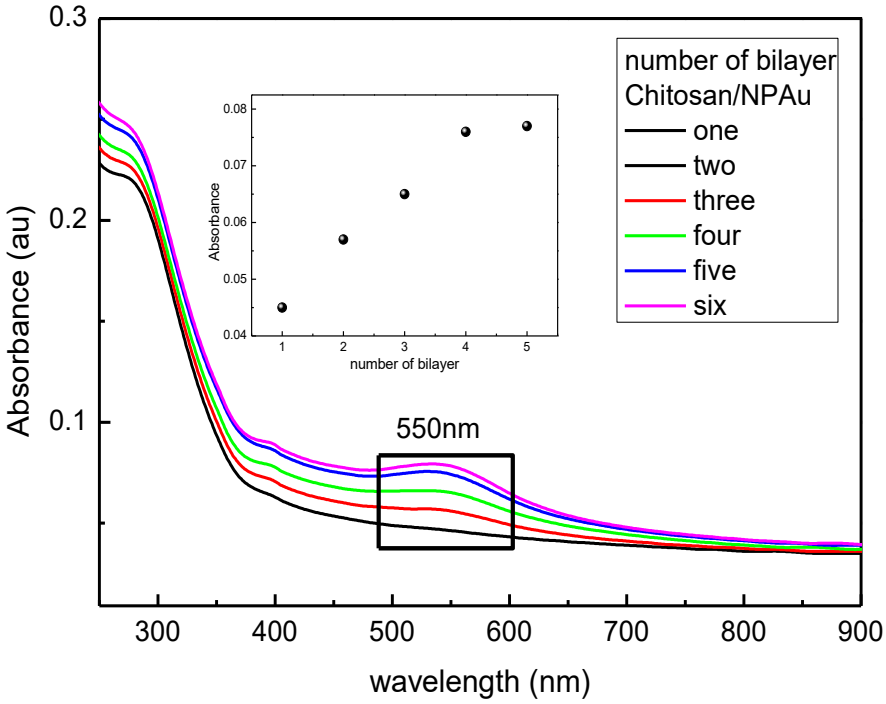

Figure S3. Absorbance spectra for Chi/AuNP-CS film growth

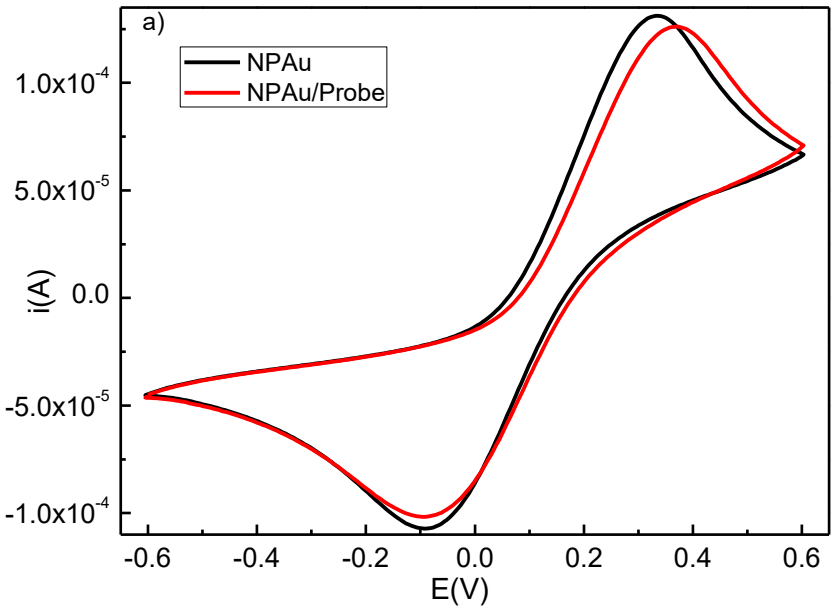

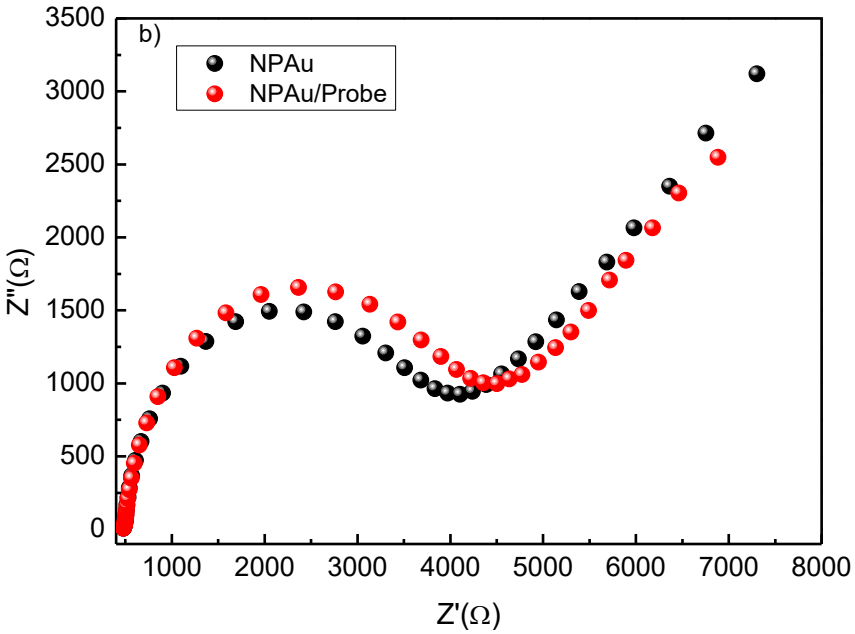

Figure S4. (a) Cyclic voltammograms of the films: AuNP-SC and AuNP-SC/Probe in the potential range between -0.6 V and 0.6V vs. ECS in $K_3Fe(CN_6)$ / $K_4Fe(CN_6)$ solution. (b) Nyquist impedance spectra from 100 kHz to 1 Hz for modified carbon electrodes with: Au NP and AuNp/Probe

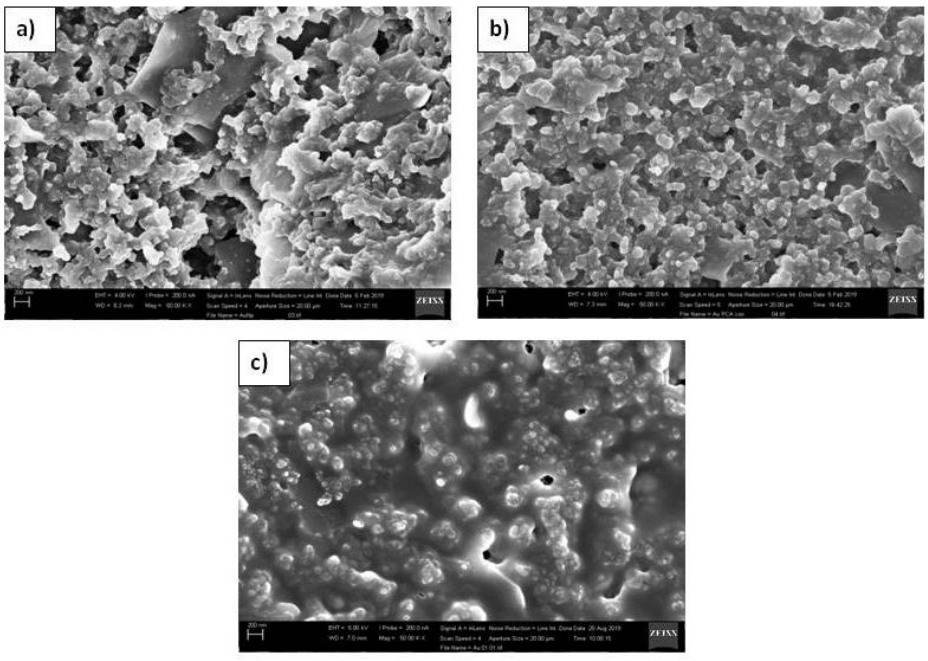

Figure S5. Scanning electron microscopy: a) AuNP-CS, b) AuNP-CS/Probe and c) AuNP-CS/Probe-DNA

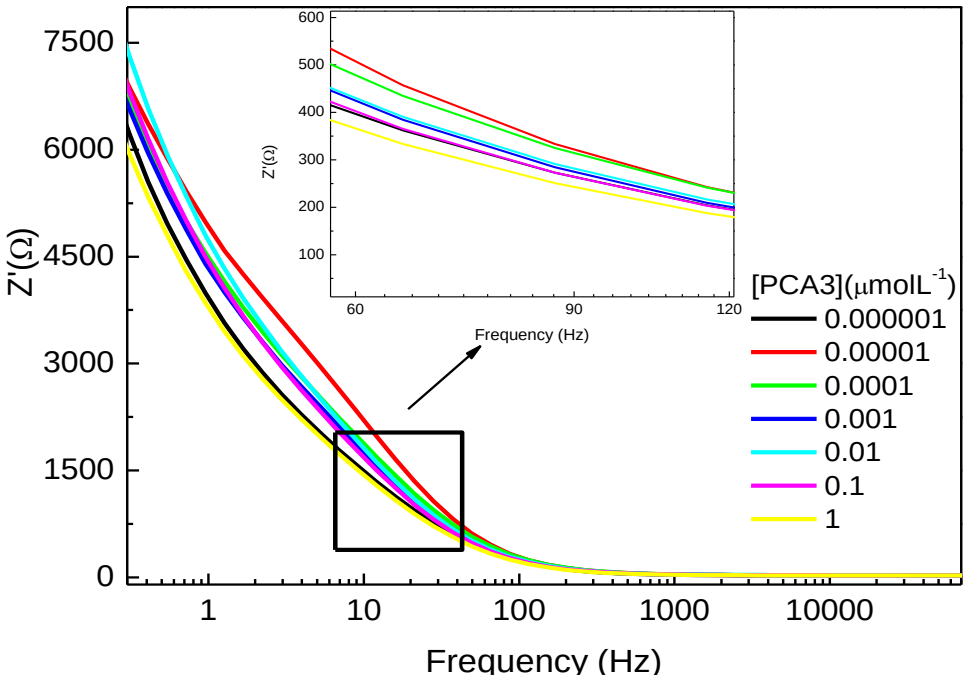

Figure S6. Impedance vs. frequency for AuNP-CS/Probe electrodes immersed in a solution of $K_3[Fe(CN)_6]$ and $K_4[Fe(CN)_6]$, with different concentrations of non-complementary sequence.

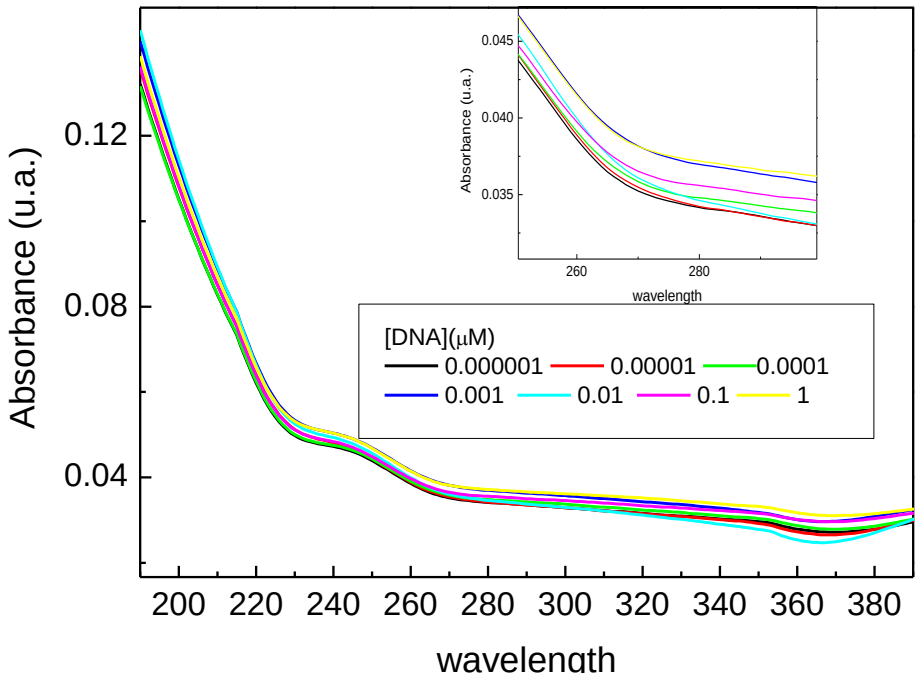

Figure S7. Absorbance spectra for AuNP-CS/Probe exposed to various concentrations of non-complementary sequencein PBS solutions.

Table S2. Characteristics of the imbalanced initial datasets generated by the segmentation of the images with a specific square window size.

Size (pixels)	Examples	Examples/class							
		n	**o**	**p_0p00001**	**p_0p0001**	**p_0p001**	**p_0p01**	**p_0p1**	**p_1p0**
300	192	12	18	24	24	24	36	30	24
200	480	30	45	60	60	60	90	75	60
100	1920	120	180	240	240	240	360	300	240

Table S3. Characteristics of the balanced datasets used in the classifications.

Size (pixels)	Examples	Examples/ Class
300	96	12
200	240	30
100	1120	140

Table S4. Accuracy obtained in the binary and multiclass classification for the dataset with windows size of 100x100 pixels.

Texture Methods	Binary			Multiclass		
	LDA	**SVM**	**1-NN**	**LDA**	**SVM**	**1-NN**
GLDM	98.6 (0.4)	98.7 (0.5)	95.3 (0.9)	77.6 (1.1)	78.7 (1.1)	46.5 (1.5)
Fourier	96.7 (0.6)	97.2 (0.5)	97.8 (0.7)	67.3 (1.1)	69.2 (1.1)	57.9 (1.7)
CNTD	98.3 (0.4)	98.2 (0.4)	89.8 (1.4)	73.3 (1.2)	75.0 (1.3)	43.7 (1.5)
Fractal	95.5 (0.7)	93.6 (0.8)	91.4 (1.3)	65.0 (1.2)	52.9 (1.2)	40.2 (1.6)
AHP	98.5 (0.5)	97.9 (0.5)	95.6 (0.8)	71.4 (1.2)	73.6 (1.3)	56.8 (1.5)
LBP	91.1 (1.4)	92.7 (1.3)	85.9 (1.3)	64.0 (1.4)	65.0 (1.4)	49.7 (1.6)
CNRNN	**99.7 (0.2)**	98.2 (0.5)	97.0 (0.7)	81.2 (1.3)	75.0 (1.3)	54.0 (1.3)
LCFNN	99.0 (0.4)	98.9 (0.4)	93.2 (0.8)	**81.5 (1.1)**	80.1 (1.4)	54.5 (1.6)

Table S5. Accuracy obtained in the binary and multiclass classification for the dataset with windows size of 200x200 pixels.

Texture Methods	Binary			Multiclass		
	LDA	**SVM**	**1-NN**	**LDA**	**SVM**	**1-NN**
GLDM	99.7 (0.5)	99.3 (0.6)	98.2 (0.8)	83.4 (2.4)	83.5 (2.3)	55.1 (3.0)
Fourier	90.2 (3.2)	99.0 (0.7)	98.7 (0.7)	65.0 (3.2)	74.7 (2.4)	65.3 (2.6)
CNTD	97.1 (1.8)	97.8 (1.0)	95.9 (1.8)	76.2 (2.3)	80.1 (2.2)	54.1 (3.2)
Fractal	98.2 (1.2)	97.2 (1.1)	96.2 (1.9)	71.3 (3.0)	61.6 (2.7)	48.0 (3.0)
AHP	95.9 (2.0)	97.9 (0.5)	97.4 (1.5)	75.0 (2.8)	80.1 (2.6)	67.5 (3.1)
LBP	95.1 (2.6)	98.8 (0.9)	90.9 (2.0)	51.9 (3.7)	73.2 (2.6)	62.8 (3.4)
CNRNN	95.4 (2.6)	99.5 (0.5)	99.0 (0.7)	71.0 (3.2)	80.4 (2.1)	65.0 (2.8)
LCFNN	99.3 (0.8**)**	**99.7 (0.4)**	99.2 (0.7)	72.7 (3.4)	**86.9 (2.2)**	72.1 (2.7)